COS Instrument Science Report 2011-01(v2)

Improved Medium Resolution Line Spread Functions for COS FUV Spectra

Gerard A. Kriss[1]

[1] Space Telescope Science Institute, Baltimore, MD

18 March 2011

ABSTRACT

We have developed an improved line spread function (LSF) for the medium resolution far-ultraviolet gratings (G130M and G160M) of the Cosmic Origins Spectrograph (COS) by taking into account scattering in the far wings due to microroughness on the HST primary mirror. We start with the preliminary model LSFs that include the broad, non-Gaussian wings caused by mid-frequency wave-front errors (MFWFEs) that are produced by the zonal polishing errors on the HST primary and secondary mirrors. Since these LSFs only extend to ±50 pixels from line center, we extend these profiles to the full width of ±100 pixels observed for geocoronal Lyα using a power law profile. We optimize the normalization and index of the power-law extension by convolving a grid of model PSFs with high-resolution STIS echelle spectra of the star Sk-155 and comparing these to on-orbit COS spectra. The best fits give a power-law index of -2.25 and show that additional light of ~3% in the extended wings is required. This low level of scattering is less than pre-launch expectations for HST, as also found by Hasan & Burroughs (1993) in longer-wavelength WFPC observations. It also implies that COS internal scattering is nearly negligible. Overall, the system as a whole has impressively low scattering. We demonstrate the improvement in our characterization of the LSFs by deconvolving the Sk 155 COS spectrum in regions of saturated interstellar absorption lines. These lines are black and saturated in the deconvolved spectra, as seen in high-resolution STIS echelle spectra of the same target. We have placed the new model LSFs online for use by COS observers in analyzing their COS spectra.

Operated by the Association of Universities for Research in Astronomy, Inc., for the National Aeronautics and Space Administration

Contents:

1. Introduction

The line-spread function (LSF) of a spectrograph characterizes how incident monochromatic light is spread with wavelength in the recorded spectrum. The dominant effect is broadening of the spectral feature by the finite resolution of the instrument. More subtle effects due to diffraction and scattering in the optics of the whole system add additional features. A preliminary analysis of the on-orbit COS LSF by Ghavamian et al. (2009) showed that the Hubble Space Telescope (HST) Optical Telescope Assembly (OTA) produces non-Gaussian wings in the LSF, and both broadens the core of the profile and lowers its amplitude. The wings are a consequence of mid-frequency wavefront errors (MFWFEs) produced by zonal polishing errors on the HST OTA. Based on models of the MFWFEs, they produced a set of wavelength-dependent LSFs that reproduce observed COS spectra well when convolved with high-resolution STIS spectra of the same target.[1]

While the model LSFs do a good job of characterizing the basic profile and integrated properties of narrow spectral features in COS spectra, science investigations that depend on characterizing the depth of saturated or nearly saturated absorption features are very sensitive to the amount of scattered light allowed by the wings of the LSF. Examples of such programs are measuring the column densities of strong interstellar absorption lines by gas in our own galaxy, or the gas in the halos or interstellar medium (ISM) of external galaxies; saturated absorption lines in the wind features of stellar spectra or outflows from AGN; saturated absorption in the intergalactic medium (IGM).

The currently modeled LSFs only extend to ±50 pixels from the line center. Given that the COS primary science aperture (PSA) has a width of 2.5 arc seconds (Dixon et al. 2010), with a plate scale in the dispersion direction of 0.0229 arc seconds per pixel for grating

[1] Both the model COS LSF produced by Ghavamian et al (2009) and the empirical COS LSF described in this paper are available on the COS Web site at:

http://www.stsci.edu/hst/instrumentation/cos/performance/spectral-resolution/

G130M, light should be present in the LSF out to a radius of 55 pixels. In fact, since the COS aperture is simply a stop in the aberrated beam of the OTA, light from outside the nominal projection of the aperture still enters the spectrograph, and the profile should extend even further.

An additional property of the HST OTA which could influence the LSF, especially at ultraviolet (UV) wavelengths, is the microroughness of the primary mirror surface. The observed on-orbit scattering properties of the HST OTA were studied by Hasan & Burroughs (1993), and they showed that scattered light due to microroughness was substantially below pre-launch predictions. It was present and measurable, however. This will introduce additional scattering to the point spread function (PSF) of the OTA, and, in principle, take light from the core of the COS LSF and redistribute it to the wings.

In this report, we will improve the characterization of the far wings of the COS LSF for the medium-resolution FUV gratings G130M and G160M by establishing an optimum width for our model of the LSFs, and investigating our understanding of the scattering properties of COS and the HST OTA.

2. Form and Width of the COS FUV LSF

Hasan & Burroughs (1993) discuss the expected functional form of the scattering due to the microroughness of the HST primary mirror. At large radii (beyond 20 Airy rings), the normalized intensity $\frac{1}{I}\frac{dI}{d\omega}$ is a power law (Brown & Burroughs 1990),

$$\frac{1}{I}\frac{dI}{d\omega} \propto \left(\frac{2\pi\theta}{\lambda}\right)^{-\beta}$$

where θ is the angular offset from the center of the image and λ is the observed wavelength. Pre-launch estimates of the scattering predicted that ~5% of the incident light would be scattered at short wavelengths due to microroughness, and that the power law would have an index of -2.16. Wide Field and Planetary Camera (WFPC) observations of an isolated star through filters F889N, F487N and F284W were used to measure the far wings of the PSF. They found that the scattered light at blue and UV wavelengths in the PSF wings were lower in amplitude compared to pre-launch predictions by a factor of ~5, and fell off more rapidly with radius, with a best-fit power-law index of $\beta=-2.5$. Even in the absence of any scattering from the mirror surface, the diffraction wings of the PSF should fall as a power law of index −3 at large radii.

The incident PSF from the OTA enters COS through the aperture stop. The FUV gratings disperse the light, correct the low-frequency errors due to spherical aberration in the HST primary, correct for astigmatism along the dispersion direction, and image the spectrum on the detector. Extracted one-dimensional spectra from the COS pipeline integrate the recorded data in the cross-dispersion dimension over 35 pixels, which is 3.5 arc seconds for G130M (at 0.1 arc sec/pixel in the Y dimension) and 3.15 arc seconds for G160M (at 0.09 arc sec/pixel). Given this integration over one dimension of the PSF, we expect that the power-law index of the scattered light contribution to the LSF will have a power-law index of −1.5 if we start with $\beta=-2.5$, as observed by Hasan and Burroughs, with a limit as steep as −2 if diffraction alone ($\beta=-3$) contributes to the wings. Given that

none of the PSF measurements of Hasan & Burroughs extend to the short wavelenths we are most interested in, however, we will explore what constraints we can set on the functional shape of the scattering wings.

The next relevant question is how far to extend the wings of the LSF. We already see that geometrically, the current LSFs have widths that are both smaller than the aperture size (which is not a hard stop), and substantially smaller than the spatial integration done in the cross-dispersion direction when extracting spectra. To select an appropriate width, we take an empirical approach. Light from geocoronal Lyα fills the COS aperture. While the COS Instrument Handbook notes that this results in a width of 114 pixels in a G130M spectrum, this is not the full extent of the profile. Figure 1 shows the base of the geocoronal Lyα emission line. Diffraction, aberrations, and scattering from all elements in the system affect what we see here. Therefore, selecting a width for our new LSFs that matches what is observed for Lyα is an appropriate assumption. As shown in the figure, we choose the inflection points at the base of the profile, which occur at ±100 pixels from line center.

Figure 1. Base of the geocoronal Lyα profile in the COS G130M spectrum of Mrk 509 (PID 12022) taken through the primary science aperture. We select ±100 pixels as the extent of the profile at zero intensity.

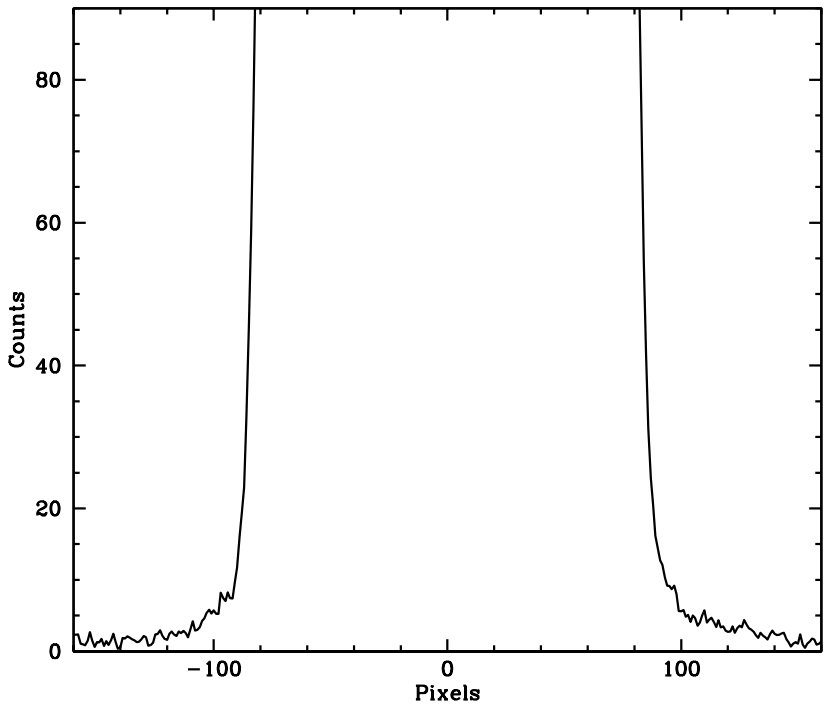

3. Optimizing the Scattering Wings of the LSF

We will assume that the scattering wings of the new LSF are power laws, but we will explore a range of spectral indices around the expected value of −1.5 to see if we can

establish any empirical constraints in the far ultraviolet. We expect microroughness from the surface of the OTA to contribute, as well as internal effects from the grating in COS, albeit at a very low level. To compute the new trial LSFs, we start with the original models that include the MWFWEs. We then extend the far wings of the LSF by adding on a power law with indices ranging from −1.0 to −2.5. For each power law index, the normalization is an additional free parameter. In our parameterization the normalization determines the transition radius–at all points beyond which the power-law extension exceeds the intensity of the original PSF, we replace the value at those points with the intensity of the power-law profile. We then integrate the new profiles and normalize the integrated intensity to unity.

To determine the best match to the COS data, we use the COS and STIS data from the SMOV calibration observations of the O9 Ib supergiant star Sk 155 in the Small Magellanic Cloud. As described in Ghavamian et al. (2009), we observed this star with COS using G130M and G160M as part of SMOV program 11489 entitled "COS FUV External Spectroscopic Performance - Part I" (PI: S. Friedman). The observation sequence and data acquisition for these spectra are described by Ghavamian et al. (2009). For this study, we used the data donwloaded from the MAST archive as processed with v2.13.6 of the COS pipeline.

Existing very high resolution observations of Sk 155 with STIS E140H (R ≈ 114,000, PID 8145, PI: D. Welty), provide "ground truth" for modeling the LSFs and matching them to the COS data. Several narrow saturated and unsaturated interstellar lines in the spectrum of Sk 155 are ideal for constraining the shape of the COS LSF. An additional STIS E140H observation of SK 155 was obtained as part of COS calibration program 12010 (PI: P. Ghavamian) to cover interstellar spectral features in the 1500–1700 Å wavelength range of the COS G160M observation. All the STIS observations used in this study were also downloaded directly from the MAST archive.

To determine the best fit for the functional form of the scattering wings on the LSF, we first resampled the STIS spectra of Sk 155 on the COS wavelength scale, either for comparison with G130M observations or G160M, depending on the wavelength range. We then convolved the STIS spectra with trial LSFs, prepared as described above, using the IRAF task noao.imred.convolve. To match these to the COS spectra, we selected spectral ranges that were dominated by a variety of narrow unsaturated and saturated ISM features. For each spectral range, we cross-correlated the convolved STIS spectra with the corresponding COS spectrum, and normalized the flux of the STIS spectrum in each spectral range to match the COS flux. We then computed χ^2 by summing over the sampled spectral range of interest:

$$\chi^2 = \sum_i \frac{(f_{COS}(\lambda_i) - f_{STIS}(\lambda_i))^2}{\sigma_{COS}(\lambda_i)^2} \quad .$$

where $f_{COS}(\lambda_i)$ is the flux in the COS spectrum at pixel i, $\sigma_{COS}(\lambda_i)$ is the error bar for the flux in pixel i, and $f_{STIS}(\lambda_i)$ is the flux in the shifted, renormalized, convolved STIS spectrum at pixel i. Table 1 shows the best-fit χ^2 for each tabulated spectral range as a function of the power-law index in our grid of trial LSFs.

Table 1: Best-fit χ^2 vs. the power-law index β. The minimum in χ^2 for each spectral range is higlighted in boldface type. The spectral ranges are given in the first column, and the number of points in each range in the second column. For reference, the third column gives the resulting χ^2 for doing the same computation with the original LSF described by Ghavamian et al. (2009).

Wavelength Range \ β	Npts	LSF0	–1.0	–1.5	–2.0	–2.25	–2.5
G130M 1189–1202	1305	4428.60	4254.48	4247.87	4179.73	4102.23	**4093.39**
G130M 1250–1263	1305	3816.90	3414.89	3401.64	3365.54	**3343.91**	3371.30
G130M 1300.25–1306.4	617	3375.25	2573.66	2473.89	**2363.27**	2422.55	2565.26
G130M 1330–1340	1004	4230.66	3537.04	3446.53	3376.06	**3331.99**	3368.16
G160M 1525–1530	409	822.30	753.32	751.13	750.53	749.69	**748.83**
G160M 1626.5–1672.2	3776	10830.78	10794.81	10773.88	10682.80	**10677.63**	10687.94

While none of the "best fits" are acceptable in a statistical sense, it is clear that the new LSFs with the extended scattering wings are preferred over the original form of the LSF. The high values of χ^2 for these fits likely result from several factors: (1) we make no flat-field corrections to the COS data; (2) we do not take the statistical errors in the baseline STIS spectra into account in our calculation; (3) the troughs of some of the saturated absorption lines in the STIS spectra have some residual issues with scattered light corrections themselves (e.g., see Valenti et al. 2002 for a discussion of corrections for scattered light in extracted STIS echelle spectra). Although our best fits show a modal preference for a power-law index of -2.25 for the scattering wings, this is only three cases out of six, with some wavelength ranges preferring either steeper or shallower wings. The variations in preferred spectral index also show no correlation with wavelength range, and the statistical significance of the variation from a uniform power-law index is also slight (given the high reduced χ^2 in each case). Therefore, we recommend adopting a power-law index of -2.25 as the preferred form of the scattering wing on the new LSF.

The new LSF with its extended scattering wings is difficult to distinguish from the LSFs in Ghavamian et al. (2009) on a linear scale. In Figure 2 we compare the new LSF for the G130M grating at a wavelength of 1200 Å to the LSF with the MFWFE corrections from Ghavamian et al. (2009) and to a simple Gaussian with a FWHM of 6.5 pixels. On the log-log scale used in Figure 2, the difference in the far wings is very obvious. As we will show below, the extra power contained in these wings is less than 3% at all wavelengths.

Figure 2. Comparison between a simple Gaussian LSF model (red line, FWHM=6.5 pixels), the LSF profile from Ghavamian et al. (2009) that includes MFWFEs from the HST OTA (blue line, calculated at 1200 Å), and the new LSF which includes power-law scattering wings of index –2.25 extending to ±100 pixels from line center.

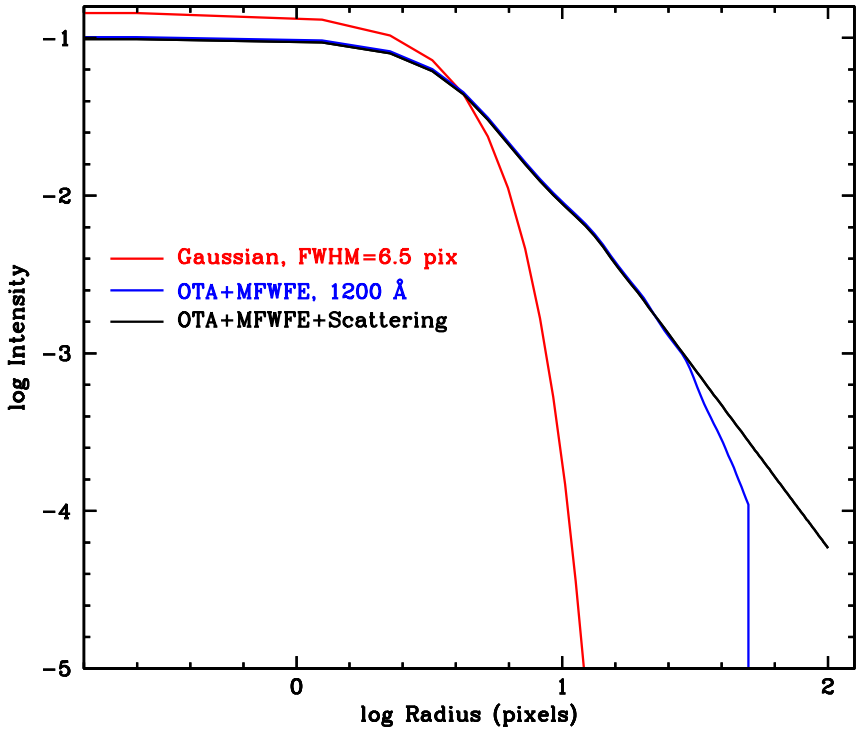

In Table 2 we give the normalization of the power-law scattering wing in each wavelength range relative to the peak of the LSF, and the radius in pixels from line center at which the power law takes over from the profile of the original LSF. As shown above in Table 1, we fit only the wavelength ranges 1175–1225 Å, 1225–1275 Å, 1275–1325 Å, 1325–1375 Å, 1525–1575 Å, 1625–1675 Å. For the wavelength regions adjacent to these, we used the closest fit in either the G130M or G160M set to choose the transition radius for the power-law extension. One can see that for each grating, this produces a smooth decrease with wavelength in the normalization of the power-law wing, just what one would expect for scattering due to microroughness on the mirror surface.

Table 2: Normalization of the power-law scattering wings on the new LSFs for each wavelength range. The peak value of the new LSF is given in the second column. The normalization of the power-law extension in the third column is relative to this peak. The fourth colum gives the transition radius (in pixels from line center) where the power-law scattering wing begins to replace the original LSF.

Wavelength Range	LSF Peak	Power-law Normalization	Transition Radius
G130M: 1125–1175	0.096	0.0249	19
G130M: 1175–1225	0.098	0.0248	19
G130M: 1225–1275	0.100	0.0244	19
G130M: 1275–1325	0.101	0.0196	21
G130M: 1325–1375	0.103	0.0171	22
G130M: 1375–1425	0.106	0.0165	22
G130M: 1425–1475	0.105	0.0160	22
G160M: 1425–1475	0.102	0.0186	22
G160M: 1475–1525	0.104	0.0178	22
G160M: 1525–1575	0.105	0.0173	22
G160M: 1575–1625	0.106	0.0169	22
G160M: 1625–1675	0.108	0.0149	23
G160M: 1675–1725	0.109	0.0144	23
G160M: 1725–1775	0.110	0.0139	23

Hasan & Burroughs (1993) note that the power-law approximation for the scattering profile due to microroughness is valid at radii beyond 20 Airy rings. At 1125 Å, the shortest wavelength in our models, this corresponds to

$$20 \times 1.22 \times (1125 \text{ Å}/2.4 \text{ m}) = 0.235 \text{ arc seconds},$$

or 10.3 pixels in a G130M spectrum. So all of our models satisfy this criterion.

Using the new best-fit forms for the LSF, we have convolved the STIS spectrum of Sk

155 and compare theses convolutions to the COS data in Figure 3 for selected spectral ranges corresponding to our fits. For comparison, we also show the convolved spectra obtained using the LSFs from Ghavamian et al. (2009). The improvement due to the new LSFs in these plots is subtle. The greatest improvement is in the depths of heavily saturated absorption lines, which is what we were expecting. Since the new LSFs have more power in the far wings due to scattering than do the original LSFs which only included the MFWFEs, we expect the scattering to fill in absorption troughs more, as one can see in Figure 3. This produces a better match to the actual COS data.

Figure 3. A series of 6 panels compares STIS E140H spectra convolved with the original LSF from Ghavamian et al. (2009) (red) to the actual COS data (black histogram) and the best fitting new LSFs that include scattering due to microroughness on the mirror (blue). The lower portion of each panel shows the difference, COS data minus convolved STIS.

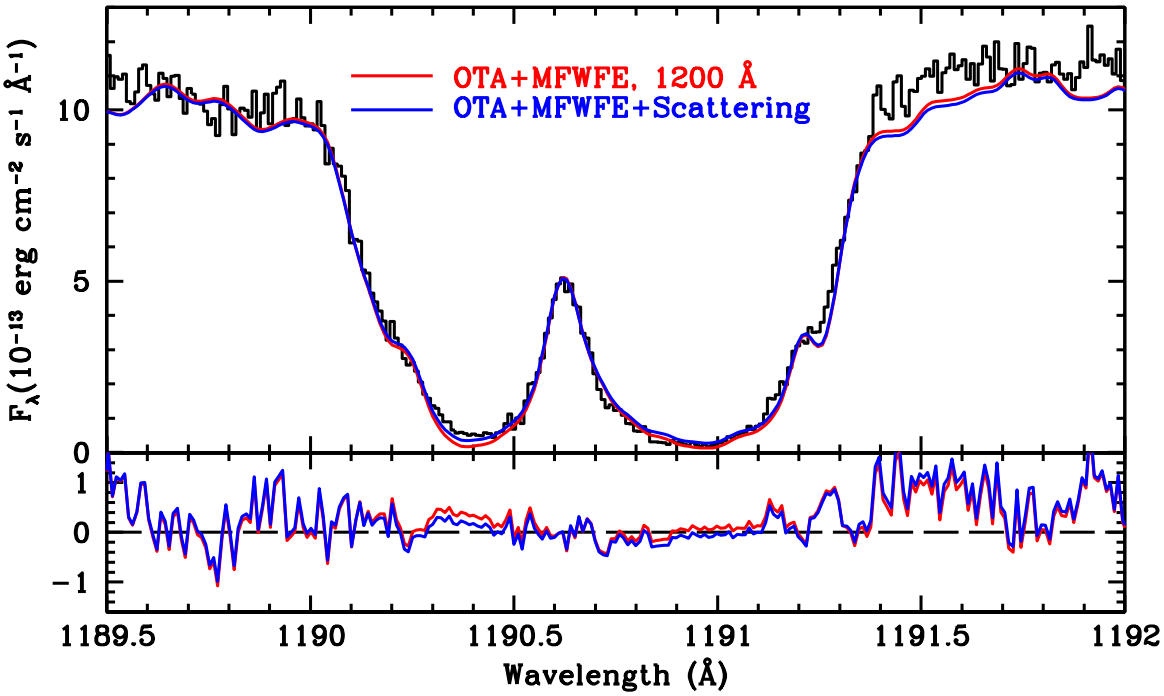

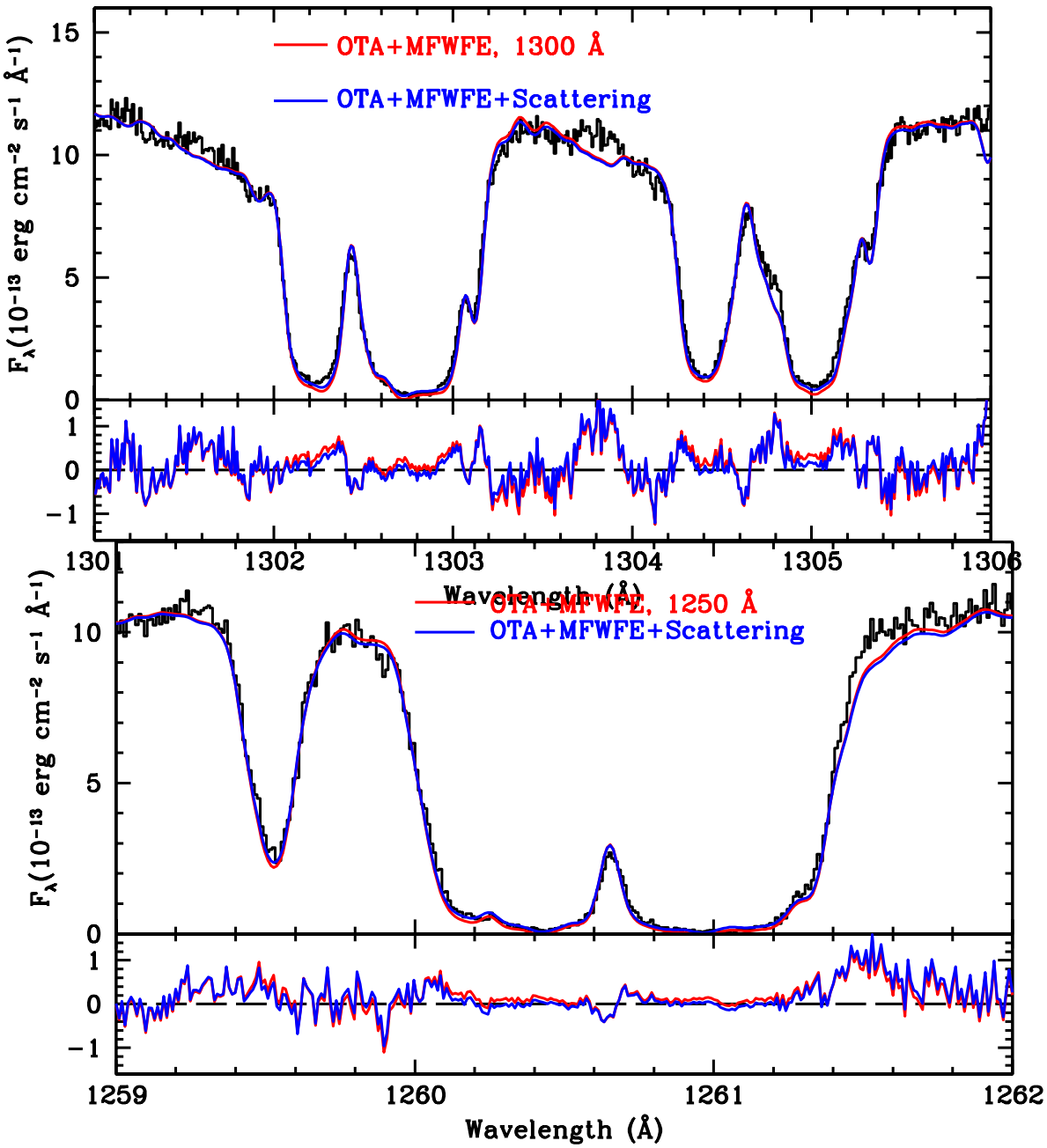
OTA+MFWFE, 1300 Å
OTA+MFWFE+Scattering
$F_\lambda(10^{-13}$ erg cm^{-2} s^{-1} Å$^{-1})$
Wavelength (Å)
OTA+MFWFE, 1250 Å
OTA+MFWFE+Scattering
$F_\lambda(10^{-13}$ erg cm^{-2} s^{-1} Å$^{-1})$
Wavelength (Å)

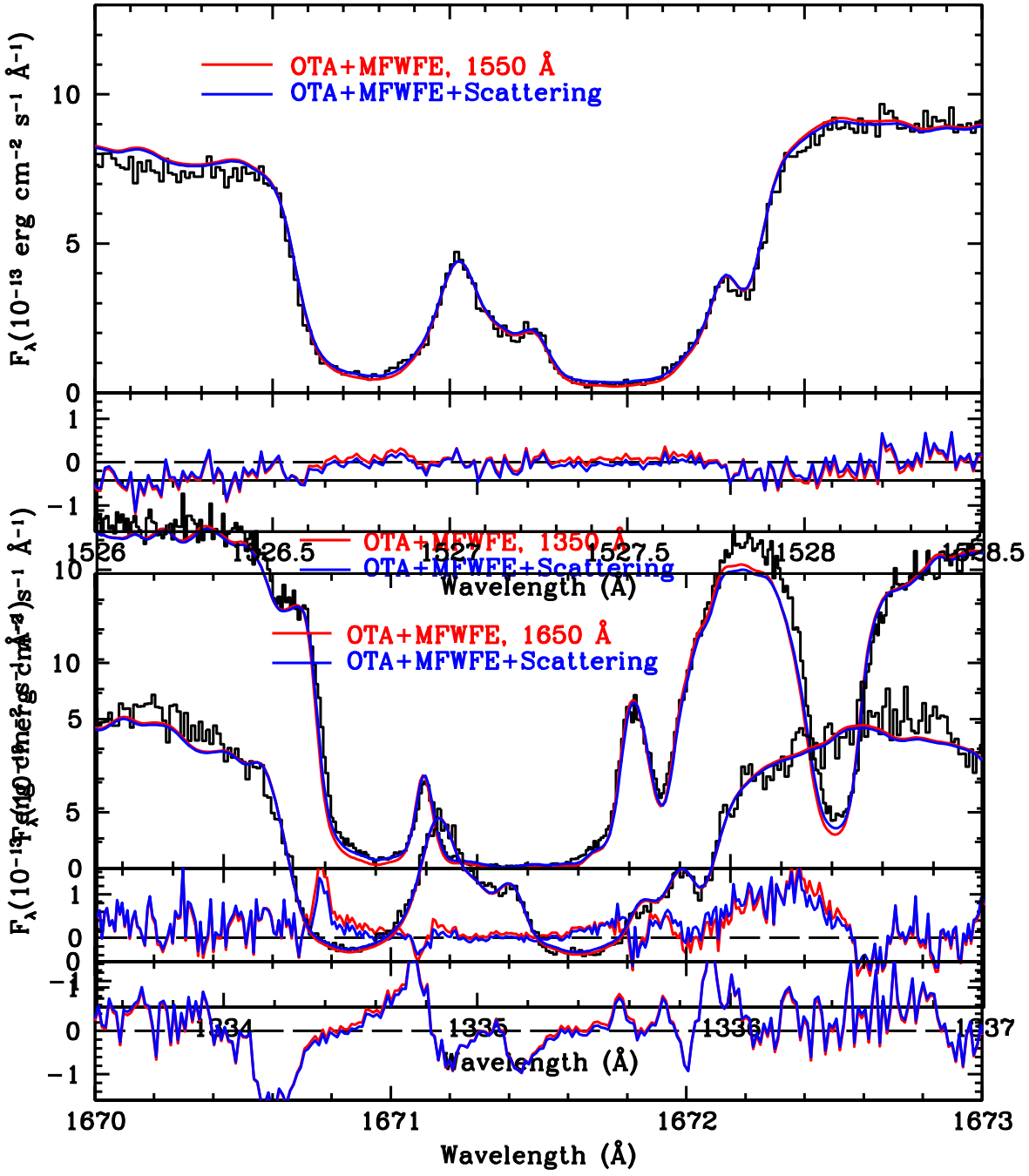
OTA+MFWFE, 1550 Å
OTA+MFWFE+Scattering
OTA+MFWFE, 1350 Å
OTA+MFWFE+Scattering
OTA+MFWFE, 1650 Å
OTA+MFWFE+Scattering
Wavelength (Å)
Wavelength (Å)

4. Quantitative Comparison of Old and New LSFs

As in the original study of the consequences of more extended line profiles in COS spectra by Ghavamian et al. (2009) that included the broadening effects of the MFWFEs from zonal errors in the HST OTA, the addition of even more extended wings to take into account scattering due to microroughness on the primary mirror indicates that even more light is lost from the core of the LSF. This will make weak, unresolved spectral features slightly more difficult to detect, and saturated absorption lines will be less black than one might have previously expected. Here we quantitatively evaluate the impact of these changes to the LSF.

Ghavamian et al. (2009) established a formal method for determining the limiting equivalent width (W) for a weak, unresolved spectral feature. For convenience, we summarize these calculations once again here.

First, we assume a known flat continuum, C_0 (cts/Å), constant in wavelength, λ. We calculate W for an absorption feature using discrete integration by summing over pixels with uniform weight:

$$W = [\sum (\Delta\lambda C_0 - N_i) / C_0)]/ f_c ,$$

where N_i is the number of counts in the ith pixel, $\Delta\lambda$ is the dispersion in Ångstroms per pixel and f_c is the fractional area of the LSF contained within the region of integration (x pixels) as a function of the number of pixels. The noise in the calculated W is then:

$$\sigma(W) = (\sum N_i)^{1/2} /(C_0 f_c).$$

To set an upper limit on a weak line, we define a significance threshold N_σ, for Gaussian-distributed errors:

$$W_{lim} = N_\sigma * \sigma(W).$$

The limiting equivalent width is then:

$$W_{lim} = N_\sigma * (\sum N_i)^{1/2} / (C_0 f_c).$$

For a very weak line, we make the approximation that the counts in each pixel are the same as in the surrounding continuum (i.e., the feature is undetected). Then,

$$\sum N_i \approx x\ \Delta\lambda\ C_0,$$

where x is the size of the region (in pixels) where the sum is peformed. Since the signal-to-noise ratio (S/N) per pixel is $\Delta\lambda\ C_0 /$ sqrt($\Delta\lambda\ C_0$), we can write:

$$W_{lim} = [N_\sigma\ \Delta\lambda / (S/N)] * [x^{1/2} / f_c (x)].$$

Thus the calculated equivalent width is a function of the size of the region chosen for the discrete integration. The ratio $[x^{1/2} / f_c (x)]$ does have a minimum, however, which we define as x_{opt}, where x is chosen to minimize the above ratio. The quantity x_{opt} is the largest

number of pixels that can be summed over a profile before the noise contributions begin to outweight the flux contributions.

We have performed the same calculations for the new LSFs with the extended scattering wings. In Table 3 we compare the quantitative properties of the "New LSFs" to the "Old LSFs" from Ghavamian et al. (2009) and to a Gaussian with a FWHM of 6.5 pixels, the nominal resolution element in a COS spectrum. In the table we compare peak intenisities, the fraction of light contained within the central core of 6.5 pixels, and the limiting equivalent widths for unresolved spectral features detected at a 3σ significance level (N_σ = 3). We assume $\Delta\lambda C_0$=100 cts/pixel for these calculations (i.e., S/N=10 per pixel). Note that as in Ghavamian et al. (2009), the tabulated results are obtained from a simple summation of counts in the absorption line, and limiting equivalent widths can likely be improved by using flux-weighted summation methods. *We find that for the new LSFs including an extended scattering wing to take into account microroughness on the surface of the primary mirror only increases the limiting equivalent width by ~3% at the shortest wavelengths*.

This minor difference is also apparent if one examines the enclosed energy for the new LSFs as a function of wavelength. In Figure 4 we show curves giving the integrated energy enclosed as a function of pixels from line center, and we compare the old and new LSFs to the curve for a simple Gaussian with a FWHM of 6.5 pixels.

Figure 4. The enclosed energy fraction of the COS LSF for an unresolved spectral feature, as measured from the center of the profile (collapsed along the cross-dispersion direction).

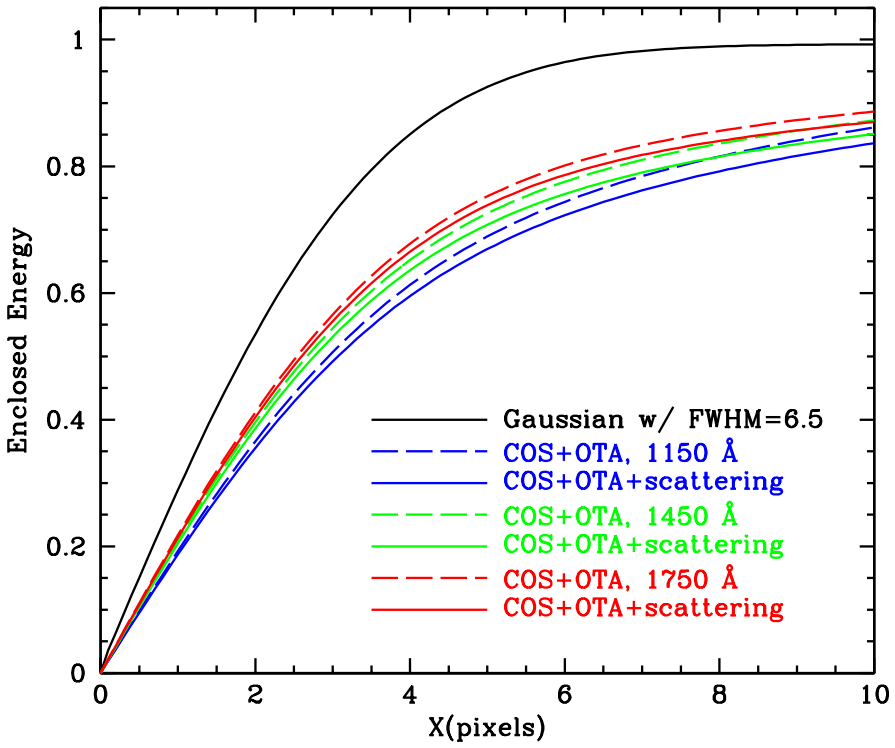

Table 3: Quantitative comparison of Old LSF (Ghavamian et al. 2009), the New LSF, and a Gaussian showing peak intensities, fraction of light within a nominal core of 6.5 pixels, and limiting equivalent widths for unresolved FUV absorption lines superposed on a bright continuum ($\Delta\lambda C_0$ = 100 cts/pixel, corresponding to S/N=10 per pixel)[1]

Grating	λ(Å)	Old LSF Peak	New LSF Peak	Old LSF Fraction within 6.5 pixels	New LSF Fraction within 6.5 pixels	Old LSF $W_{lim}(3\sigma)$ (mÅ)	New LSF $W_{lim}(3\sigma)$ (mÅ)
G130M	GAUSS	0.1445	0.1445	0.761	0.761	9.9	9.9
G130M	1150	0.0990	0.0961	0.536	0.521	13.7	14.1
G130M	1200	0.1013	0.0984	0.545	0.530	13.5	13.9
G130M	1250	0.1026	0.0997	0.551	0.535	13.4	13.8
G130M	1300	0.1042	0.1013	0.557	0.541	13.3	13.7
G130M	1350	0.1067	0.1038	0.566	0.551	13.1	13.5
G130M	1400	0.1085	0.1057	0.574	0.559	13.0	13.3
G160M	GAUSS	0.1445	0.1445	0.761	0.761	12.1	12.1
G160M	1450	0.1047	0.1020	0.565	0.550	16.1	16.5
G160M	1500	0.1067	0.1041	0.572	0.558	15.9	16.3
G160M	1550	0.1075	0.1051	0.575	0.562	15.9	16.2
G160M	1600	0.1086	0.1063	0.579	0.567	15.8	16.1
G160M	1650	0.1099	0.1077	0.585	0.573	15.6	15.9
G160M	1700	0.1116	0.1095	0.593	0.582	15.4	15.7
G160M	1750	0.1120	0.1099	0.598	0.587	15.3	15.6

[1]*The table columns are (1) the FUV grating chosen, (2) indication of a gaussian LSF or of the modeled wavelength for the on-orbit LSF, (3) the peak intensity of the Old LSF (Ghavamian et al. 2009; normalized to an area of unity), (4) the peak intensity of the New LSF, (5) the fraction of the Old LSF area contained within the nominal resolution element for COS of 6.5 pixels, (6)) the fraction of the New LSF area contained within 6.5 pixels, (7) the calculated limiting equivalent width for a 3σ detection feature for the Old LSF, (8) the limiting equivalent width for a 3σ detection feature for the New LSF.*

5. Implications for the Scattering Properties of the OTA and COS

As we noted earlier, Hasan & Burroughs had expected that scattering due to microroughness on the HST OTA would have produced a power-law wing on the PSF with an index of –2.16. Their observations of the far wings of the PSF in WFPC observations showed that the observed scattering was substantially lower in amplitude (by a factor of several) and steeper, with an index of –2.5. All of their observations were also at longer wavelengths than we have measured here, with the shortest wavelength in their observations being 2480 Å. Our results here imply that even at the shortest wavelengths observable with HST that scattering due to microroughness is minute, amounting to 3% or less of the total light. Our best-fit power law index for the LSF of –2.25 also implies that the index on a full PSF would be –3.25, even steeper than that found by Hasan & Burroughs, and steeper than the profile due to diffraction alone. The only way that the

profile can be physically steeper is due to vignetting by the entrance aperture. This implies that actual scattering is negligible. We note that this is also an upper limit on OTA performance since our measured profiles must include some scattering internal to COS itself. As noted by Shull et al. (2010), scattering internal to COS, as well as its background, is extremely low. All in all, the system as a whole has impressively low scattering.

6. Application of the New LSFs to Deconvolution

Given the minor impact of these changes, one might ask whether the new LSFs have any practical utility. Since all the differences are in the far wings of the LSF, the greatest consequence will be for scientific investigations that rely on high contrast between bright continua and deep absorption troughs. In cases like this, the scattering wings of the LSF will take light from the continuum and transfer it to any adjacent absorption trough that is within ~100 pixels. So any deep absorption features that are 100–200 pixels in width will be contaminated with continuum light.

A good way to see the utility of the new LSFs presented here is to deconvolve the COS spectra we have been using in this study to show directly the impact that the LSFs have on the spectrum. As a test, we used a Lucy-Richardson deconvolution on the COS spectra of Sk 155 as implemented in the routine "lucy" in the IRAF package stsdas.analysis.restore. Lucy requires observations in counts since it calculates its statistical information for errors directly from the data itself, so we converted the Sk 155 spectra back to counts before using lucy. Background is negligible in the Sk 155 spectra, so the variance for each data point in the spectrum are the count data themselves. After supplying the LSF to lucy, the only remaining tunable parameter is the number of iterations. We found that 15–20 iterations converged on a good result. (More iterations tended to amplify noise in the continuum.) After deconvolution, we converted the count spectrum back to flux for comparison to the higher-resolution STIS spectrum. In Figure 5 we show the result for a deconvolution of the G130M spectral region from 1189.5–1192 Å (which was shown in its original form in the first panel of Figure 3). The figure compares the COS spectrum deconvolved with the new LSF to the STIS spectrum, and we also show the result of deconvolving the COS spectrum with old LSF. One can see the noticeable improvement that the new LSF provides in matching the saturated troughs of the Mg I absorption lines in this spectrum–the saturated line centers in the spectrum deconvolved with the new LSF are totally black (flux equals zero), but the spectrum deconvolved with the old LSF still shows a small amount of residual flux in the troughs. One can see a similar improvement in the cores of the saturated Si II lines in the 1250 Å spectrum in the second panel of Figure 5.

Figure 5. Two panels compare deconvolved COS data using the new LSFs (blue curves) to the STIS E140H spectra (black histograms). COS data deconvolved with the original LSF from Ghavamian et al. (2009) (red curves) are not completely black at line center.

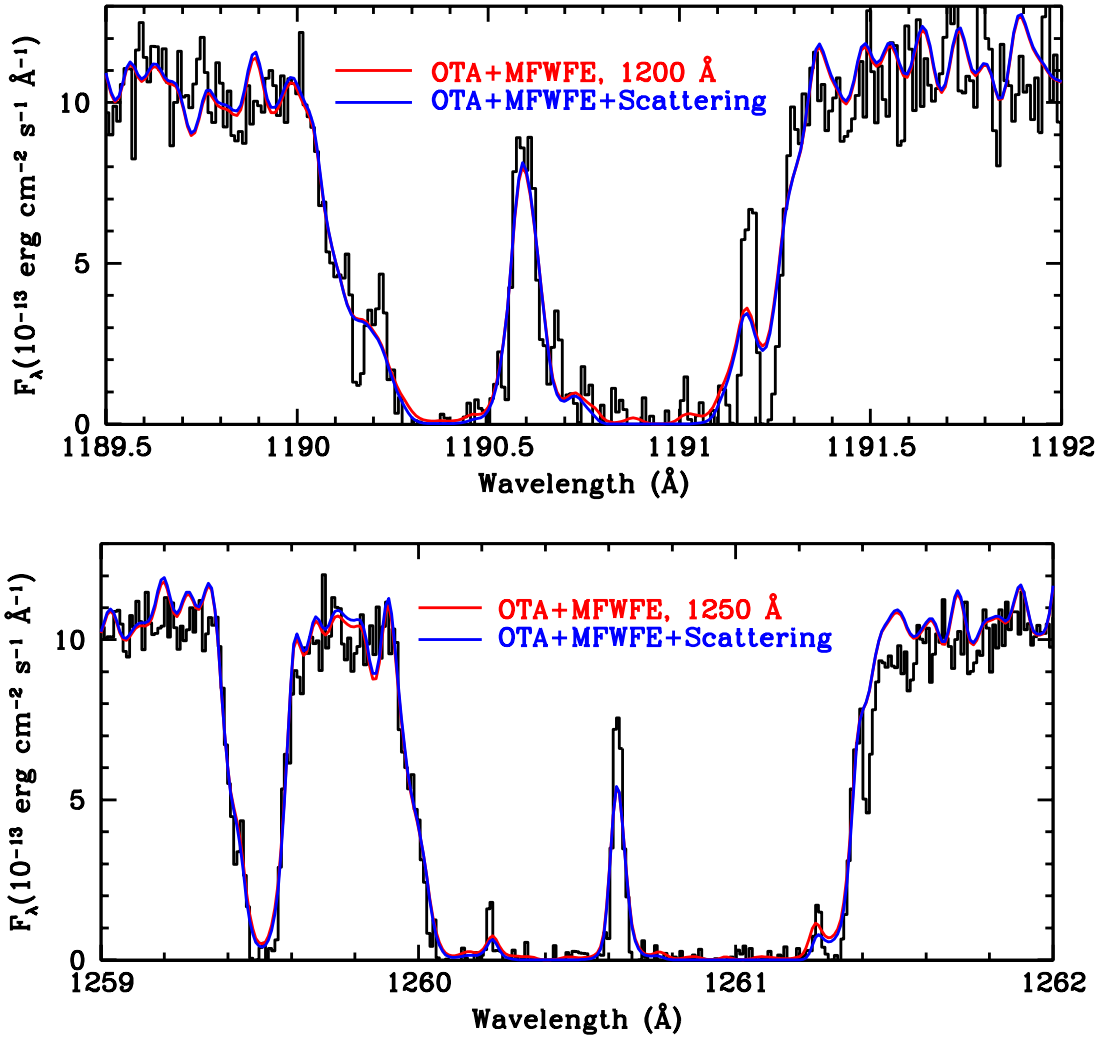

7. Summary

We have developed improved LSFs for the COS medium resolution far-ultraviolet gratings (G130M and G160M) by empirically measuring the possible shape of far wings on the LSF. These could be due to simply the r^{-3} wings of the PSF simply due to diffraction, plus scattering due to microroughness on the HST primary mirror and the COS grating itself. We start with the preliminary model LSFs from Ghavamian et al. (2009) that include the broad, non-Gaussian wings caused by mid-frequency wave-front errors (MFWFEs) that are produced by the zonal polishing errors on the HST primary and secondary mirrors. Since these preliminary LSFs only extended to ±50 pixels from line center, we extend these profiles to the full width of ±100 pixels observed for geocoronal Lyα. The profile extension

is characterized by a power law. We optimize the index and normalization of the power-law extension by convolving a grid of model PSFs with high-resolution STIS echelle spectra of the star Sk 155 and comparing these to on-orbit COS spectra. Pre-launch expectations for HST anticipated scattering due to microroughness of ~5% with a power-law slope of -2.16 (Hasan & Burroughs 1993) for the wings of the PSF. Our best-fit power-law index of -2.25 for the LSF implies a PSF index of −3.25, which is even steeper than normal diffraction, which is plausible due to vignetting of the PSF by the COS entrance aperture. The best fits show that additional light of only ~3% in the extended wings is required. The extremely low scattering we find here is similar to the results of Hasan & Burroughs at longer wavelengths using WFPC, and it implies very low levels of actual scattered light internal to COS or due to the HST OTA. Nevertheless, these low-level wings improve the characterization of the LSF. We demonstrate the improvement by deconvolving the Sk 155 COS spectrum in regions of saturated interstellar absorption lines. These lines are black and saturated in the deconvolved spectra, as seen in high-resolution STIS echelle spectra of the same target. We have placed the new model LSFs online for use by COS observers in analyzing their COS spectra.

Change History for COS ISR 2011-01

Version 1: 18 March 2011 - Original Document
Version 2: 30 March 2023 – link updated

References

Brown, R. A., and Burroughs, C. J. 1990, Icarus, 87, 484

Dixon, W. V., et al. 2010, "The Cosmic Origins Spectrograph Instrument Handbook, Version 3.0", (Baltimore, STScI)

Ghavamian, P., et al., "Preliminary Characterization of the Post-Launch Line Spread Function of COS", COS ISR 2009-01(v1), (Baltimore, STScI)

Hasan, H. & Burrows, C. J. 1993, SPIE 1945, 36

Shull, J. M., et al. 2010, ApJ, 722, 1312

Valenti, J., et al. 2002, "2-D Algorithm for Removing Scattered Light from STIS Echelle Data", STIS ISR 2002-01, (Baltimore, STScI)

Welty, D. E., Lauroesch, J. T., Blades, J., Hobbs, L. M. & York, D. G. 2001, ApJ 554, L75

Acknowledgements

I thank George Hartig for helpful discussions on the scattering properties of the HST optics, and Cristina Oliveira and Parviz Ghavamian for their feedback on the draft document.